J MATER RES TECHNOL. 2020;9(2):1286–1295

Available online at www.sciencedirect.com

jmr&t

Journal of Materials Research and Technology

www.jmrt.com.br

Original Article

Influence of microstructure and porosity on the fracture toughness of Al-Si-Mg alloy

Maria Teresa Di Giovanni [a,*], *João T. O. de Menezes* [b,c], *Emanuela Cerri* [a], *Enrique M. Castrodeza* [c]

[a] Department of Engineering and Architecture, University of Parma, Parco Area Delle Scienze 181/A, 43124 Parma, Italy

[b] Department of Metallurgical and Materials Engineering, COPPE/Federal University of Rio de Janeiro, 21941-972 Rio de Janeiro, Brazil

[c] Department of Mechanical Engineering, Polytechnic of Milan, Via La Massa 1, 20156 Milano, Italy

ARTICLE INFO

Article history:
Received 26 November 2018
Accepted 20 November 2019
Available online 24 December 2019

Keywords:
A356 aluminum alloy
Fracture toughness
J-R curves
Porosity
Microstructure
Hardness.

ABSTRACT

With improving molten metal quality and foundry technology, cast alloys are expected to be used more commonly in critical applications. The demands for improved damage tolerance of cast aluminum alloys have increased the importance of fracture-related properties. In this perspective, the present study aims to evaluate the effect of four different aging treatments on fracture toughness of a die cast A356 Al alloy with and without Cu addition. Crack growth resistance curves (*J*-R curves) were experimentally evaluated using the ASTM E1820-17 standard procedure on 25 mm thick compact tension C(T) specimens. The influence of microstructure and porosity in hardness and fracture toughness (J_{Ic}) is discussed. In addition, microstructural observations were carried out to endorse the fracture mechanisms.

1. Introduction

The past two decades have been marked by great progress and innovation in the aluminum foundry industry. However, the low ductility and fracture toughness, as compared to the wrought aluminum alloys counterpart, still represent one of the major impediments for increased use of aluminum casting in the aerospace industry [1]. Increasing efforts to improve both the melt quality and process condition [2] are being made and, as a result, Al-Si alloys are expected to be used more commonly in critical application areas. So far, the lack of knowledge towards the fracture toughness of these alloys had limited their use to field where fracture-related properties were not relevant. Though, fracture toughness evaluation in Al-Si alloys might represent a key step to understand the metallurgical features which control the toughness and hence will might allow proper material specifications to be settled for those applications where fracture-related failure must be prevented. In this concern, previous studies [3] reported the fracture toughness of a series of Al-Si castings and defined a ratio (λ/DE_{Si}) where λ is the silicon particle spacing and DE_{Si} is the equivalent silicon particle diameter. Tirakiyoglu [4] examined the fracture toughness potential of cast Al-7%Si-Mg alloys as a function of yield strength. Tohgo and Oka [5] focused on

* *Corresponding author.*
E-mail: mariateresa.digiovanni@unipr.it (M.T. Giovanni).

https://doi.org/10.1016/j.jmrt.2019.11.055

Table 1 – Chemical compositions (wt.%) of A356 reference alloy and Cu-added A356 alloy.

Alloy	Si	Mg	Fe	Cu	Ti	Sr	Al
A356 (reference)	6.624	0.216	0.086	0.006	0.103	< 0.001	bal.
A356 + 1 wt.% Cu	6.915	0.262	0.091	0.983	0.086	< 0.001	bal.

the influence of coarsening treatment of the fracture toughness of Al-Si-Mg alloys. Lee et al. [6] investigated the effect of the Si-particles on the fracture toughness of A356 alloy cast, using different casting technologies. The comprehensive conclusion rising up from these studies is that the resistance to crack growth increases with enhancing the degree of refining of dendrite cells and eutectic silicon. Comparing the casting processes, the crack tip plasticity is higher in slowly solidified microstructure (sand castings) and lower in permanent mold or, die casting. Hence, the factors favoring the fracture toughness would be decreased dendritic cell size and refinement of Si-eutectic and intermetallic, the opposing factor would be reduced plasticity due to increase in yield strength, both due to primary cell and eutectic refinement. Further, the influence of minor chemical modification has been analyzed by Alexopoupolos [1]. However, as reported by Staley [7] there are several extrinsic factors such as porosity, oxides and inclusions that tend to affect the fracture toughness of these class of alloy.

In this framework, the present work proposes a study on the fracture toughness of a A356 Al alloy and its Cu-containing (1 wt.%) variants, under for different aging conditions. The toughness values were evaluated through crack growth resistance curves (J-R curves) which were determined by the unloading compliance method. The effect of porosity, Secondary Dendrite Space Arming (SDAS) and eutectic Si particles morphologies on the fracture toughness results (J_{Ic}) were analyzed. In addition, microstructural observations were carried out to endorse the fracture mechanisms.

2. Materials and methods

2.1. Materials

The compositions of the studied alloys as measured by optical emission spectrometry are listed in Table 1. They were prepared in laboratory so as to contain different populations of porosity. The castings were obtained with a gravity die casting process using a copper mold of 65×103×40 mm^3. Aiming to collect a wide range of SDAS variety, specimens for fracture testing were sectioned from different zones in the casting ingot. Four different heat treatments were applied, details and related specimen codes are presented in Table 2.

2.2. Fracture testing

Fracture toughness tests were performed according to ASTM E1820-17 standard [8] on fatigue pre-cracked C(T) specimens with nominal dimensions as shown in Fig. 1 and initial a_0/W ratios close to 0.5. Fatigue pre-cracking and fracture tests were made in air at room temperature using an MTS Landmark servo-hydraulic machine instrumented with ±25 kN load cell and an MTS 632.03F-31 fracture extensometer positioned at the crack mouth. Crack lengths along the tests were estimated by unloading compliance method through the compliance solution given by the ASTM E561-15a standard for C(T) specimens [9]:

Table 2 – Cast Al alloys, heat treatment conditions, and specimen codes.

Cast Al alloy	Heat treatment	Specimen code
A356	5 h at 530 °C +2 h at	Ref 2_190
A356 + 1 wt.% Cu	190 °C	1Cu 2_190
A356	5 h at 530 °C +4 h at	Ref 4_190
A356 + 1 wt.% Cu	190 °C	1Cu 4_190
A356	5 h at 530 °C +4 h at	Ref 4_155
A356 + 1 wt.% Cu	155 °C	1Cu 4_155
A356	5 h at 530 °C +10 h at	Ref 10_155
A356 + 1 wt.% Cu	155 °C	1Cu 10_155

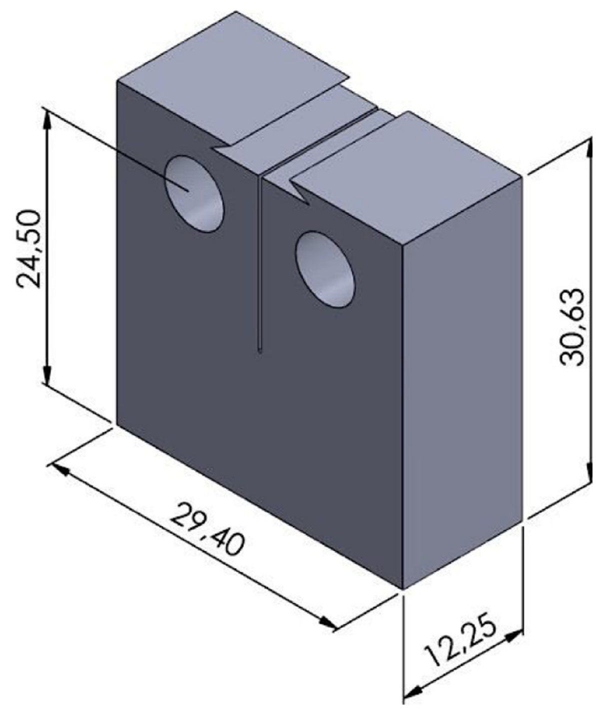

Fig. 1 – Compact-tension C(T) test specimens. Main nominal dimensions (in mm).

$$\frac{a}{W} = 1.0010 - 4.6695u + 18.460u^2 - 236.82u^3 + 1214.90u^4 - 2143.6u^5, \quad (1)$$

where

$$u = \frac{1}{1 + \sqrt{E\acute{B}C_i}}. \quad (2)$$

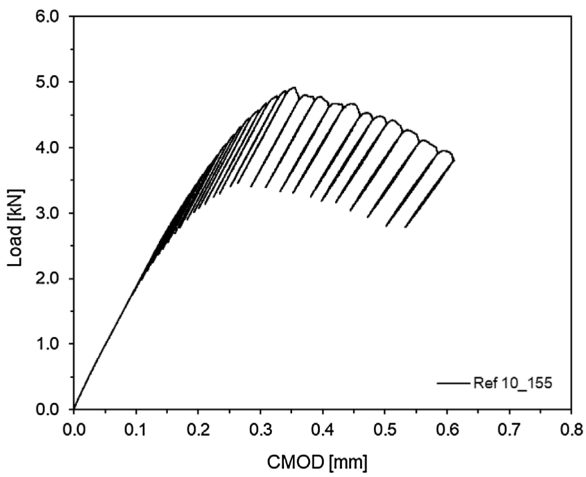

Fig. 2 – Typical experimental P-CMOD record for the Ref 10_155 C(T) specimen.

Table 3 – Initial and final physical crack lengths, and initial a_0/W ratio of the tested specimens.

Specimen	a_0 (mm)	a_f (mm)	a_0/W
Ref 2_190	12.84	16.67	0.52
1Cu 2_190	12.57	17.10	0.51
Ref 4_190	12.86	16.25	0.53
1Cu 4_190	12.86	16.70	0.52
Ref 4_155	12.85	15.72	0.53
1Cu 4_155	12.91	16.20	0.53
Ref 10_155	12.02	15.71	0.49
1Cu 10_155	12.87	16.64	0.53

For plane strain conditions, the appropriate effective elastic modulus is $E' = E/(1-\upsilon^2)$. B is the specimen thickness and C_i is the compliance evaluated at the crack mouth (C_i = ΔCMOD/ΔP).

2.3. Hardness tests

Vickers hardness tests (HV) were conducted with a Leica VMHT micro Vickers tester with a load of 500 gf and a dwell time of 15 s, according to the UNI EN ISO 6507 specification [10]. Further hardness examinations were performed with a load of 25 gf with the aim of testing the sole aluminum α- matrix.

Table 4 – Individual J_{Ic} values and Vickers hardness for the investigated alloys.

Specimen	J_{Ic} (kJ/m^2)	$HV_{500\ gf}$	$HV_{25\ gf}$
Ref 2_190	9.4	97.92 ± 1.82	97.06 ± 3.03
1Cu 2_190	8.2	89.94 ± 4.98	94.67 ± 4.12
Ref 4_190	8.3	94.72 ± 1.78	94.27 ± 2.88
1Cu 4_190	10.9	94.32 ± 2.73	99.19 ± 2.01
Ref 4_155	16.9	84.60 ± 5.93	70.29 ± 2.78
1Cu 4_155	14.7	83.67 ± 7.96	65.94 ± 1.95
Ref 10_155	9.3	92.00 ± 3.51	82.99 ± 2.57
1Cu 10_155	9.4	86.55 ± 6.09	94.87 ± 3.29

Table 5 – SDAS, porosity and Si particles characteristics for each tested specimen.

Specimen	SDAS (μm)	Porosity		Si particles	
		% area	ED (μm)	AR	ED (μm)
Ref 2_190	47.4 ± 5.6	2.09	14.87	1.44	2.82
1Cu 2_190	56.4 ± 6.1	3.93	70.49	1.80	4.39
Ref 4_190	61.0 ± 4.5	1.91	52.14	1.53	3.18
1Cu 4_190	34.3 ± 4.1	0.92	25.03	1.54	3.81
Ref 4_155	58.3 ± 5.1	0.97	15.95	1.48	2.97
1Cu 4_155	69.6 ± 7.9	2.89	25.16	1.90	3.62
Ref 10_155	57.4 ± 7.3	1.69	32.34	1.48	3.52
1Cu 10_155	52.1 ± 6.4	2.66	24.73	1.92	4.30

2.4. *Microstructural analysis*

Samples for microstructural analyses were cut from the fractured tested specimens about 10 mm below the fracture surface, embedded in phenolic resin and prepared using standard grinding and polishing procedures. Microstructure analyses were performed using a Leica DMi8 polarized light optical microscope (OM). Quantitative metallography was carried out using the LAS image analysis software. A measurement field was systematically defined by composing 8–12 frames at a magnification of 250×. Percentages of pore area (PA) were calculated as the ratio between 'analyzed pores surface area (μm^2)' and 'total analyzed surface area (μm^2)', while equivalent circle diameter (ED) were measured following the procedures described in [11]. Eutectic Si particles characteristics such as aspect ratio (AR) and equivalent circle diameter (ED) were also measured following the procedures described

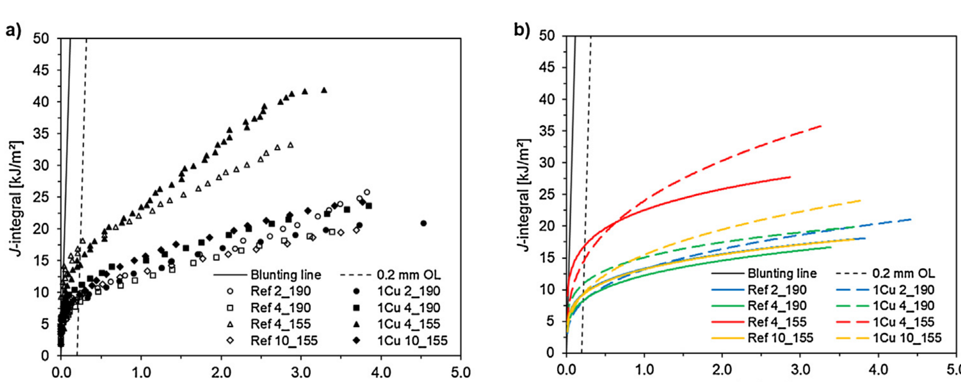

Fig. 3 – a) Experimental J-Δa pairs for the tested specimens. b) Theoretical adjusted J-R curves for the tested specimens.

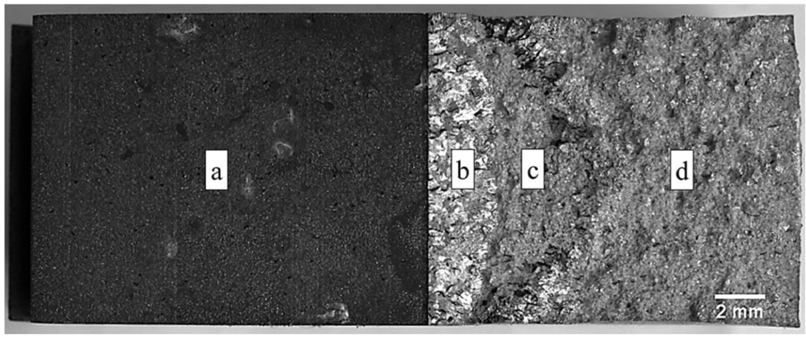

Fig. 4 – Fracture surface of the C(T) specimen Ref 4_155 showing the EDM notch (a), the fatigue pre-crack (b), the stable crack growth (c) and the fatigue post-crack (d).

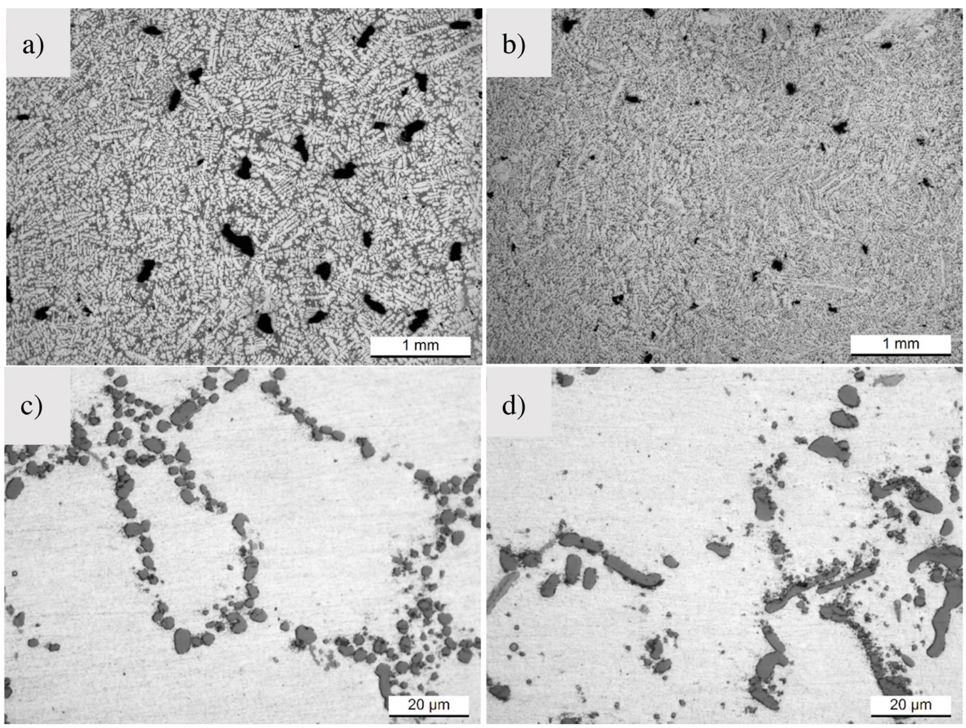

Fig. 5 – Representative population of porosity in the Ref 2_190 specimen of A356 alloy (a) and in the 1Cu 4_190 specimen of Cu-added A356 alloy (b). Eutectic Si Particles in the Ref 2_190 specimen of A356 alloy (c) and in the 1Cu 2_190 specimen of Cu-added A356 alloy (d).

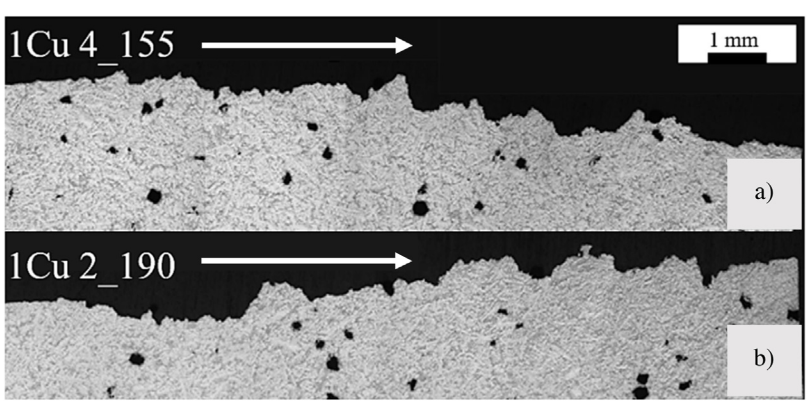

Fig. 6 – Crack paths of two representative C(T) specimens. a) specimen 1Cu 4_155, and b) specimen 1Cu 2_190. The arrows indicate the crack growth.

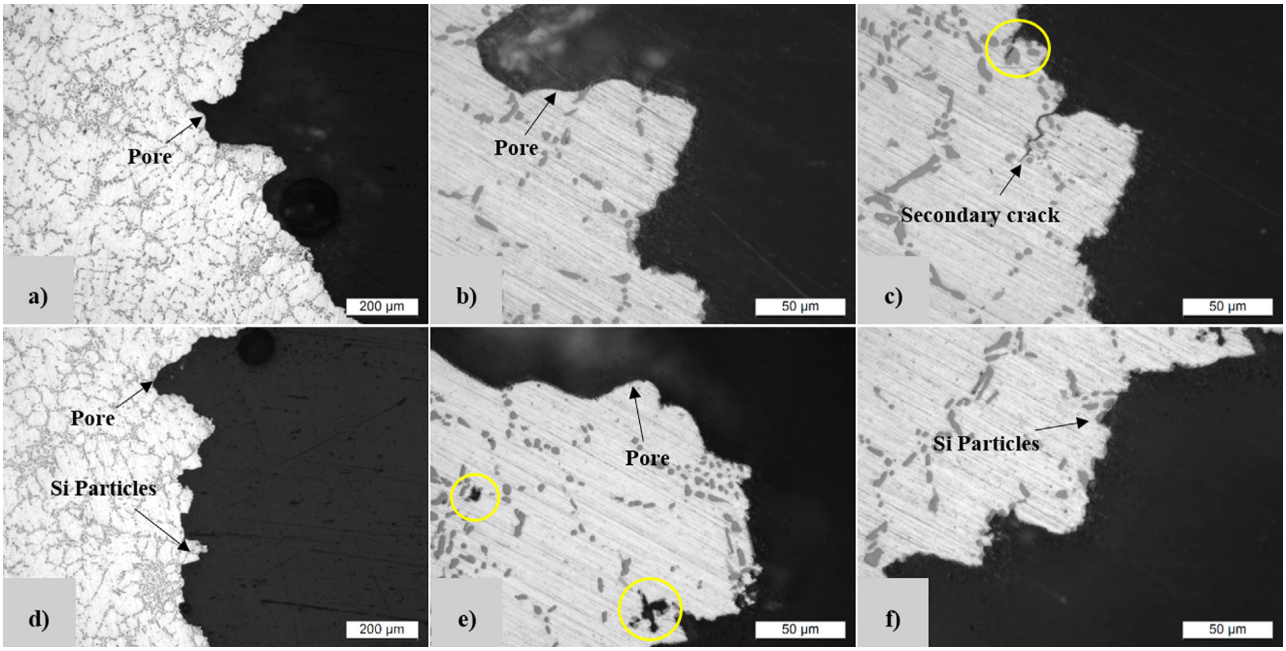

Fig. 7 – Details of the region of stable crack propagation of two representative C(T) specimens. a–c) specimen 1Cu 4_155, and d–f) specimen 1Cu 2_190.

in [11]. SDAS measurements were performed using the line intercept method, over 10 fields at 50× magnification.

2.5. *Fracture surfaces analysis*

Fracture surfaces were observed with a ZEISS ULTRA 55 field emission scanning electron microscopy (FE-SEM). Element mapping were obtained through energy dispersive X-ray spectroscopy (EDS), operated at an acceleration voltage of 20 kV.

3. Results and discussion

3.1. *P-CMOD records*

Fig. 2 features the typical experimental load (P) *vs.* crack mouth opening displacement (CMOD) record for the tested C(T) specimens. In this case, the experimental record of Ref 10_155 C(T) specimen is presented. The unloading-reloading sequences necessary for crack length measurements by the elastic compliance technique can be clearly seen.

3.2. *J-R curves*

Fig. 3-a summarizes the J-Δa pairs of points of the eight investigated specimens sorted by open or filled symbol as a function of the chemical composition, and by different symbols as function of the heat treatment condition. In its turn, Fig. 3-b presents all the theoretical adjusted J-R curves. Auxiliary lines according to ASTM E1820-17 were also plotted in both figures. It can be observed that while most of the curves are found to be grouped in the same area in the plot, the Ref 4_155 and 1Cu 4_155 featured higher J-R curves, indicating higher fracture toughness and the role of the heat treatment.

3.3. *Fracture surface and crack lengths measurements*

After the fracture tests, specimens passed through a fatigue post-cracking in order to mark the extension of stable crack growth. Fig. 4 shows a typical fracture surface of the tested specimens. From left to right, the EDM notch, the fatigue pre-crack, the stable crack growth, and the fatigue post-crack regions can be clearly identified in the image.

Initial and final physical crack lengths were measured from fracture surfaces according to BS 7448-1:1991 standard [12]. Table 3 presents initial (a_0) and final (a_f) crack lengths measurements as well as the initial a_0/W ratio of each specimen.

3.4. *Fracture toughness and Vickers hardness*

Table 4 presents the fracture toughness values (J_{Ic}) and Vickers hardness (HV_{500gf} and HV_{25gf}) of each specimen tested. The fracture toughness was calculated as recommended by the ASTM 1820-17 standard, taking the interception between the theoretical adjusted J-R curve and the line parallel to the blunting line at an offset value of 0.2 mm.

3.5. *Metallographic analysis*

The microstructural features examined in this analysis encompasses: SDAS, pore area percentage, porosity equivalent diameter (ED), eutectic silicon particle aspect ratio (AR) and equivalent silicon particle diameter (ED). A list of the experimental results is given in Table 5. Representative examples are presented in Fig. 5-a and Fig. 5-b. With reference to characteristics of the eutectic Si particles, it is possible to observe an overall increase in the eutectic ED size in the Cu-containing alloys as compared to reference A356 alloy. Additionally, the former case offers coarse (higher ED) and acicular (higher AR)

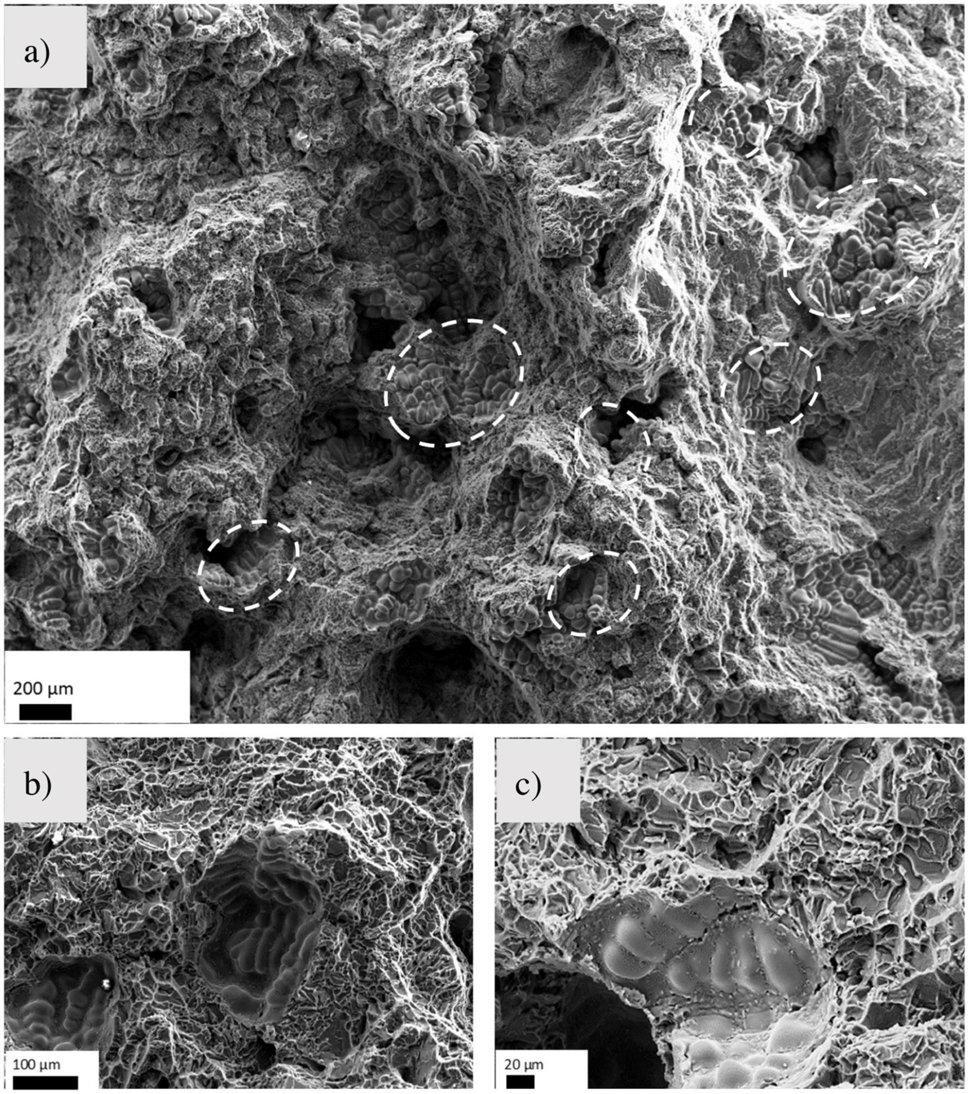

Fig. 8 – SEM images of fracture surface showing typical casting defects. Specimen 1Cu 4_155.

Si particles, where the A356 alloys present a fine and well-spheroidized eutectic network (Fig. 5-c and Fig. 5-d).

3.6. *Fractographic observations*

Fig. 6 shows the crack paths for the two representative Cu-containing samples aged under different conditions: a) aged 4 h at 155 °C and b) aged 2 h at 190°. Further insights of microstructural features leading the crack are presented in Fig. 7. The cracks preferably extend along solidification cells, where eutectic Si particles are mainly segregated and easily connected by the crack, playing an easy path role for stable crack growth. In addition, some cracked eutectic Si particles are pointed out in the images of Fig. 7-c and Fig. 7-d. Shrinkage porosities are also present at the crack paths.

Fig. 8-a and Fig. 8-c are representative fractographies of the 1Cu 4_155 specimen, taken at different magnification. Higher magnifications images (Fig. 8-b and Fig. 8-c) reveal a fracture surface typical of ductile mechanisms. Fracture surfaces have been deeply investigated as reported in Fig. 9. Aiming to clearly evidence both the α-Al matrix (in red) and the eutectic Si particles (in green), EDS maps of Al and Si have been provided. Microcracks within the Si particles are clearly observed in both the Cu-added (Fig. 9-c) and the A356 reference (Fig. 9-e) alloys. In accordance with Table 5, Si particles in the A356 reference alloy appear smaller (lower ED) and more spherodized (lower AR) as compared to the Cu containing alloy. The most of cracked Si particles are observed along the interdendritic regions, where they mainly segregated and easily connected to play a bridging role. Moreover, shear bands observed in both the investigated alloys (please see Fig. 9-c to Fig. 9-f) reveal the matrix influence on the crack propagation.

3.7. *Fracture toughness correlations*

Based on previous study proposed by Lee et al. [6], that exploited the fracture mechanism of A356 alloy through in-situ SEM analysis, lower local fracture driving force micro-cracks seem to be initiated at the eutectic Si particles in interdendritic regions (Figs. 7 and 9). With the increasing of

J MATER RES TECHNOL. 2020;9(2):1286–1295

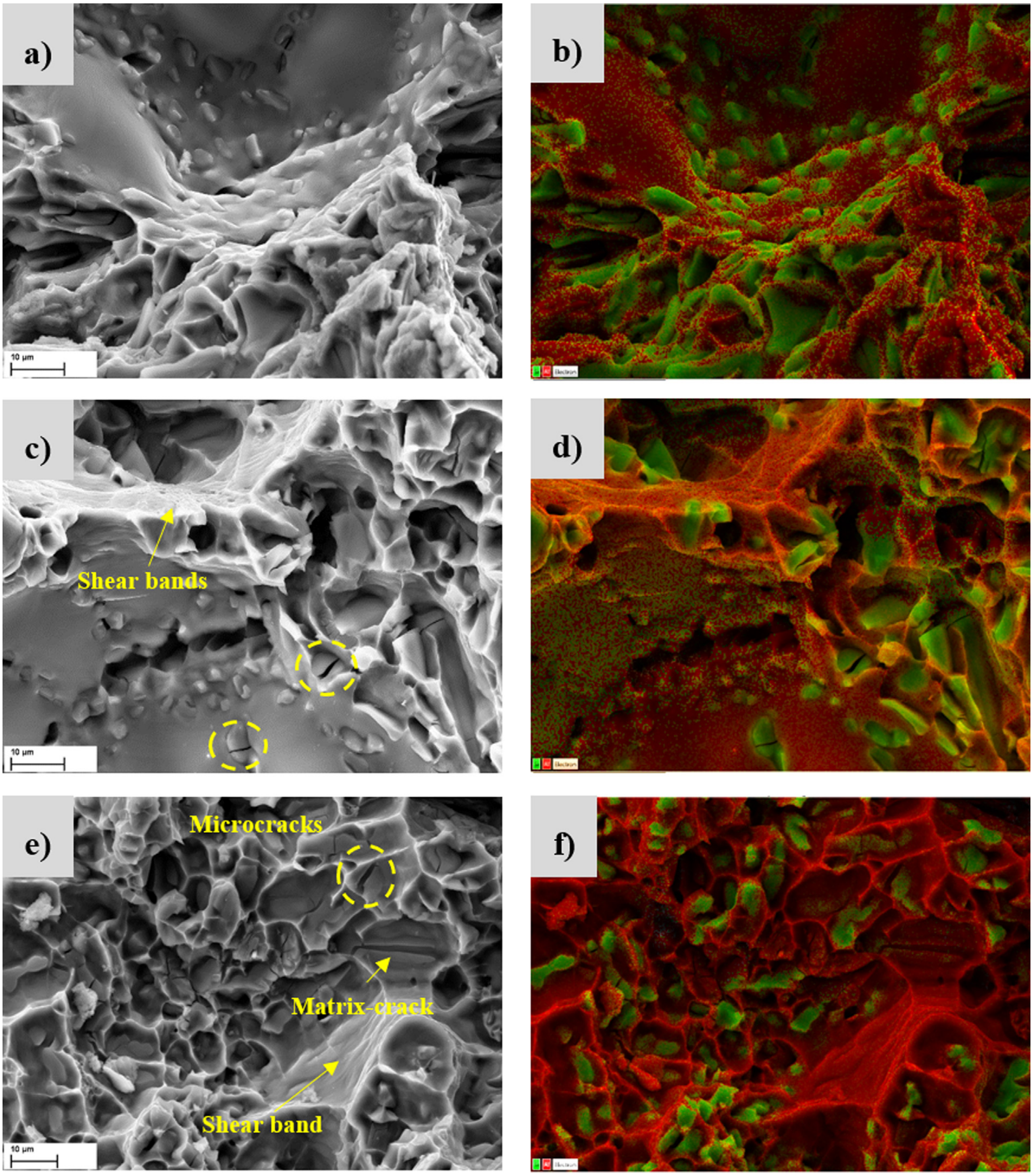

Fig. 9 – SEM images of fracture surfaces and EDS maps of Al and Si. a) to d) specimen 1Cu 4_155, e) and f) specimen Ref 4_190.

local driving force, crack grows by conventional ductile mechanisms associated to the metallic matrix, as suggested by the shear bands in Fig. 9-c and 9-e.

From the microstructural point of view, the material's crack growth resistance is known to be influenced by porosity and the solid phase microstructure (eutectic network + α-Al matrix). Although the effect of porosity on fracture toughness is well known [13], other factors influence the fracture toughness. In order to understand the influence of microstructural features observed in these alloys, the effects of equivalent porosity diameter and the microstructural characteristics were focused, as follows.

3.7.1. *The effect of porosity and hardness on fracture toughness*

First, it is important to note the significant presence of shrinkage pores in all casted alloys. In order to evaluate the influence of porosity, the fracture toughness values were plotted as function of the equivalent porosity diameter for each specimen (Fig. 10-a). Generally speaking, and considering all results

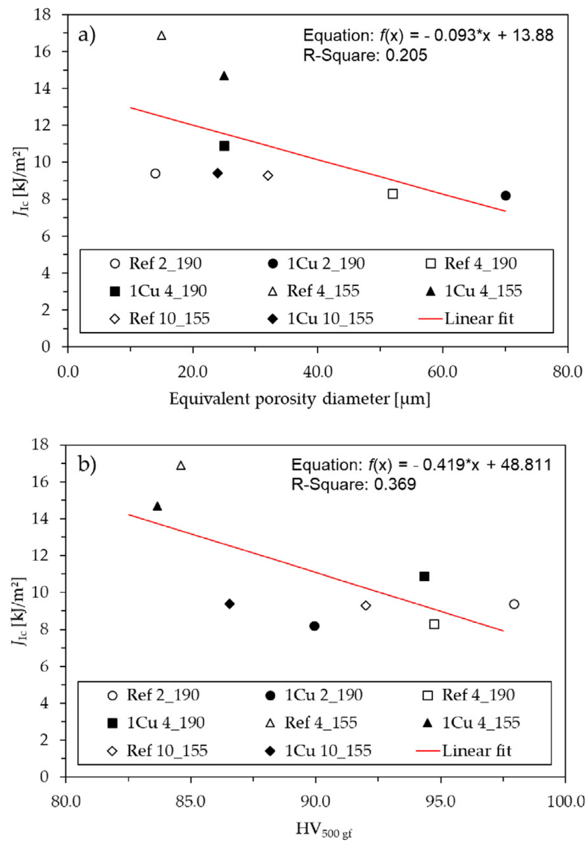

Fig. 10 – Fracture toughness correlation between (a) equivalent porosity diameter and (b) 500 gf Vickers hardness.

there is a visible tendency. The fracture toughness increases with decreasing in porosity equivalent diameter. The highest fracture toughness values were obtained for the specimens that were heat treated for 4 h at 155 °C; these samples also presented small porosity equivalent diameter values (~ 20 µm), but not the lowest, indicating that the fracture toughness is also influenced by other microstructural characteristics that have been modified by the heat treatment.

The Cu-addition influence on the porosity can be evaluated from Table 5. Except for the alloy heat treated by 4 h at 190 °C, the Cu-containing alloys presented a higher percentage porosity. The effect of Cu on porosity in Al-Si alloy with 0.1%Fe is discussed in [14]. On the other hand, the influence of Cu-addition does not present an effective influence on the porosity equivalent diameters. Shrinkage and gas porosity casting defects depend on a lot of variables, including chemical composition, but in this case no influences could be verified.

When J_{Ic} values are plotted against the $HV_{500\,gf}$ results (Fig. 10-b) the fracture toughness decay as hardness values increase, as expected. The lowest hardness values and the highest J_{Ic} values were measured for the specimens that were heat treated by 4 h at 155 °C. As can be observed in Fig. 10-b, the Cu-addition resulted in lower hardness values considering each heat-treatment. However, the 1 % Cu alloys were not the toughest in all cases, meaning that other microstructural features influence the fracture toughness.

As proposed by Seideffine [15], the addition of Cu is found to promote the formation of coarse Si particles, and to enlarge the solidification interval, increasing the shrinkage porosity. Voids formed at the interfacial separation between eutectic Si particles and the aluminum α-matrix are not observed in the alloys investigated. This suggest a good particle-matrix interfacial strength, own to the presence of Si within the matrix [16]. It is possible to presume that the load transfer is mainly supported by the Si particle-matrix interface, and that the shear-lag type strengthening effect [17] plays a crucial role in the increased strength due to eutectic Si particles. Hence, if considering the alloy investigated as composite material where the α-Al phase is the matrix that needs to be reinforced, while the network of eutectic Si particles compounds is the stronger phase acting as a reinforcement [18], it is possible to understand the hardness response reported in Table 5, that show a decrease in HV with adding Cu. The finer and uniform are the eutectic Si particles distributions, the higher is the reinforcement achieved.

3.7.2. *The influence of eutectic Si particles and SDAS*

According to Lee et al. [6], the A356 + 1 wt.% Cu alloys that have coarser eutectics Si particles are expected to offer higher J_{Ic} values as compared to the Reference A356 alloys. In this case, as shown in Fig. 11, fracture toughness and silicon particles equivalent diameter (ED) are not so easily correlated, this is probably due to the porosity effect which has overruled the effect of the Si particles size.

Fig. 12 features the fracture toughness *vs.* Si particles aspect ratio (AR). As can be seen, although coarsened and less spheroidized eutectic microstructures are present in all the 1 wt.% Cu alloys if compared to the Reference alloys, no overall effect on the fracture toughness was detected. However, Fig. 12 (b) presents the fracture toughness *vs.* Si particles AR for all data taking away the specimens that were heat-treated for 4 h at 155 °C. Analyzing this data, it is possible to observe a tendency: the fracture toughness increases as the Si particles AR decreases. The same tendency can be observed analyzing the heat-treated specimens for 4 h at 155 °C separately (upper part of the Fig. 12 (a)).

In the Fig. 13 fracture toughness was plotted as function of the SDAS. Analyzing the results for each individual heat treatment, a clear tendency can be observed: the fracture toughness increases with decreasing SDAS. The same tendency can be observed analyzing all data pairs without the heat-treated specimens for 4 h at 155 °C, as can be seen on Fig. 13 (b). That could be explained by the relation between SDAS and the equivalent Si particles diameter. As SDAS decreases with the solidification rate [19] the Si particle equivalent diameter decreased too, and the fracture toughness increase. According to the experimental results the Cu content did not affect SDAS in that case.

4. Concluding remarks

In this work, the effect of four different aging treatments on the fracture toughness of a die cast A356 Al alloy with and

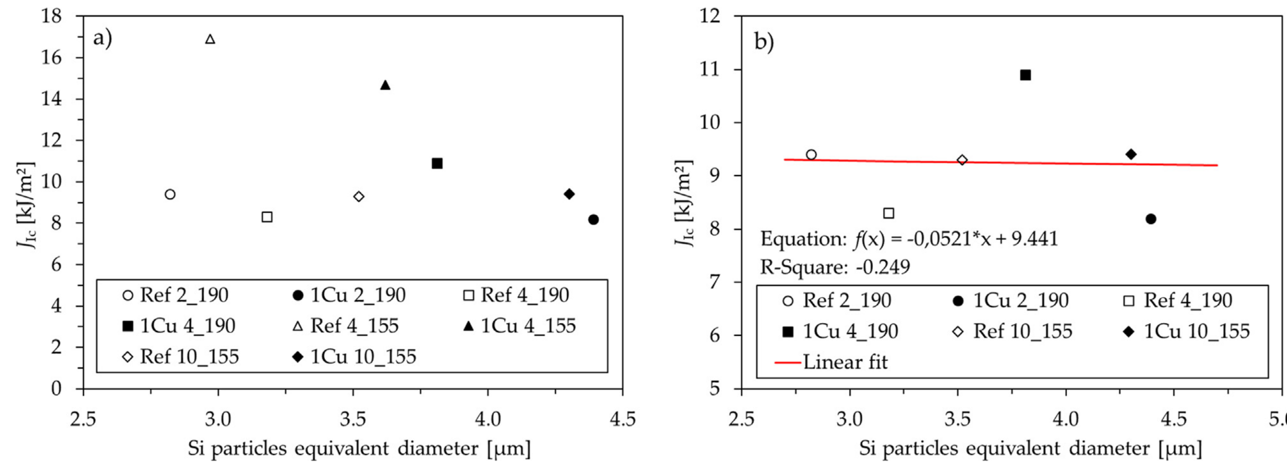

Fig. 11 – Fracture toughness *vs.* Si particles equivalent diameter (ED). In (a) for all data results and in (b) without the data results of the heat-treated specimens by 4 h at 155 °C.

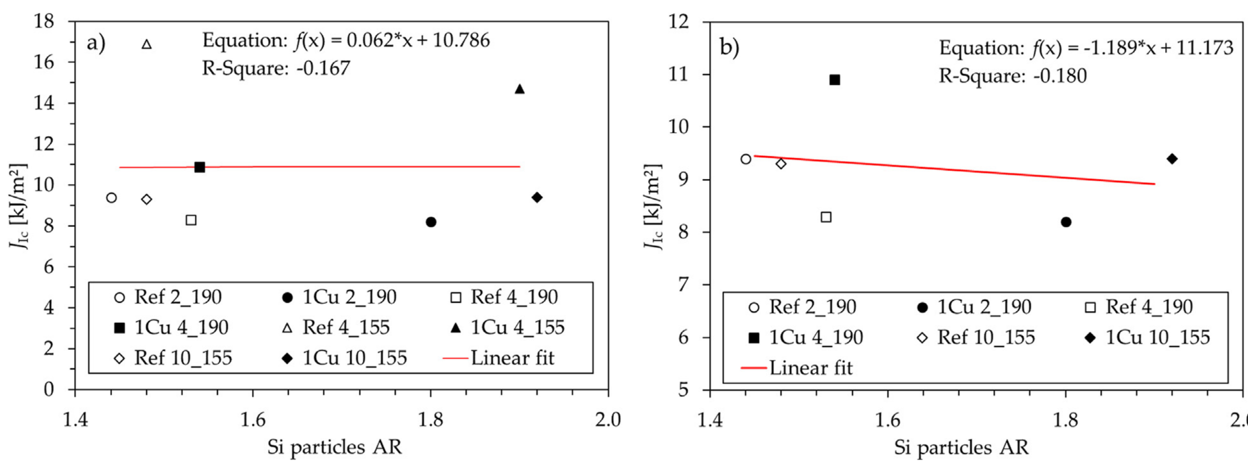

Fig. 12 – Fracture toughness *vs.* Silicon particles aspect ratio (AR). In (a) for all data results and in (b) without the data results of the heat-treated specimens by 4 h at 155 °C.

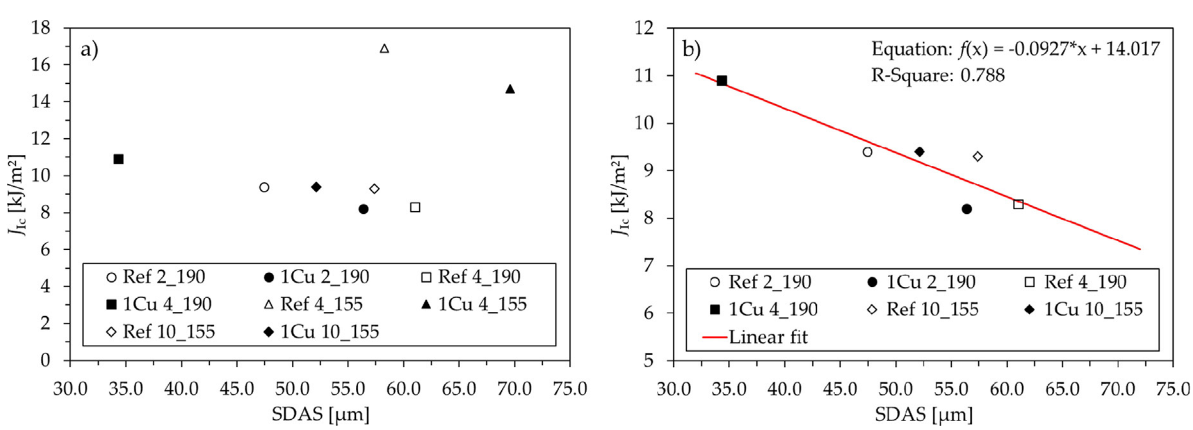

Fig. 13 – Fracture toughness *vs.* SDAS. In (a) for all data results and in (b) without the data results of the heat-treated specimens by 4 h at 155 °C.

without Cu addition was evaluated. Crack growth resistance curves (*J*-R curves) were experimentally measured and the influence of microstructure and porosity on hardness and fracture toughness (J_{Ic}) was discussed. In summary, the following remarks can be drawn:

- The fracture process was related to the presence of eutectic Si particles in interdendritic regions. The cracks preferably extend along solidification cells, where eutectic Si particles are mainly segregated and easily connected by the crack, playing an easy path role for stable crack growth.

- If compared to the A356-Reference alloys, the A356 Cu-containing alloys showed higher J-R curves. In other words, Cu-containing alloys will feature higher resistance to fracture after the onset of stable crack growth.
- For the A356 Al alloy in those studied conditions, the fracture toughness increases as the equivalent porosity diameter and the HV_{500g} hardness decreases. In the same way, the fracture toughness increases as Si particle AR and SDAS decreases.
- For the heat treatments performed in this work, the aging at 155 °C for 4 h optimized the J_{Ic} in the alloy with and without 1% wt. Cu addition. This result seems to be independent by any microstructural features examined in this paper, resulting more an expression of the precipitation condition.

Conflict of interest and authorship conformation form

- All authors have participated in (a) conception and design, or analysis and interpretation of the data; (b) drafting the article or revising it critically for important intellectual content; and (c) approval of the final version.
- This manuscript has not been submitted to, nor is under review at, another journal or other publishing venue.
- The authors have no affiliation with any organization with a direct or indirect financial interest in the subject matter discussed in the manuscript

REFERENCES

[1] Alexopoulos ND, Tiryakioğlu M. Relationship between fracture toughness and tensile properties of A357 cast aluminum alloy. Metall Mater Trans A 2009;40A:702–16.

[2] Anilchandra AR, Arnberg L, Bonollo F, Fiorese E, Timelli G. Evaluating the tensile properties of aluminum foundry alloys through reference castings – a review. Materials 2017;10:1011–23.

[3] Hafiz MF, Kobayashi T. Fracture toughness of eutectic Al-Si casting alloy with different microstructural features. J Mater Sci 1996;31:6195–200.

[4] Tirayakioglu M. Fracture toughness potential of cast Al-7%Si-Mg alloys. Mater Sci Eng A 2008;497:512–4.

[5] Tohgo K, Oka M. Influence of coarsening treatment on fatigue strength and fracture toughness of Al-Si-Mg alloy castings. Key Eng Mater 2004;261–163:1263–8.

[6] Lee K, Kwon YN, Lee S. Effects of eutectic silicon particles on tensile properties and fracture toughness of A356 aluminum alloys fabricated by low-pressure-casting, casting-forging, and squeeze-casting processes. J Alloys Compd 2008;461:532–41.

[7] Staley JT. Microstructure and toughness of high-strength aluminum alloys. ASTM STP 1976;605:71–96.

[8] ASTM E1820-17a. Standard test method for measurement of fracture toughness. West Conshohocken, PA: ASTM International; 2017.

[9] ASTM E561-15a. Standard test method for K-R curve determination. West Conshohocken, PA: ASTM International; 2015.

[10] ISO 6507: 2018. Metallic materials – vickers hardness test. International Organization for Standardization; 2018.

[11] Lattanzi L, Di Giovanni MT, Giovagnoli M, Fortini A, Merlin M, Casari D, et al. Room temperature mechanical properties of A356 alloy with Ni additions from 0.5 wt to 2 wt%. Metals 2018;8:224–39.

[12] BS. 7448 Part 1: method for determining of K_{Ic}, critical crack tip opening displacement (CTOD) and critical J values of fracture toughness for metallic materials under displacement controlled monotonic loading at quasistatic rates. London: British Standards Institution; 1991.

[13] Srinivasan M, Seetharamu S. Fracture toughness of metal castings, science and technology of castings processes, chapter 10, IntechOpen; 2012. p. 285–312.

[14] Dinnis CM, Taylor JA, Dahle AK. Porosity formation and eutectic growth in Al-Si-Cu-Mg alloys containing iron and manganese. In: Nie JF, Morton AJ, Muddle BC, editors. Proc. 9th int. Conf. On aluminium alloys. Institute of Materials Engineering Australasia Ltd; 2004. p. 1016.

[15] Seifeddine S, Sjölander E, Bogdanoff T. On the role of copper and cooling rates on the microstructure, defect formations and mechanical properties of Al-Si-Mg alloys. Mater Sci Appl 2013;4:171–8.

[16] Poruks P, Yakubtsov I, Boyd JD. Martensite-ferrite interface strength in low-carbon bainitic steel. Scr Mater 2006;54: 41–5.

[17] Nardone VC, Prewo KM. On the strength of discontinuous silicon carbide reinforced aluminum composites. Scr Metall 1986;20:43–8.

[18] Asghar Z, Requena G, Boller E. Three-dimensional rigid multiphase networks providing high-temperature strength to cast AlSi10Cu5Ni1-2 piston alloys. Acta Mater 2011;59:6420–32.

[19] Okayasu M, Ota K, Takeuchi S, Shiraishi T. Material properties of cast aluminium alloys produced by various casting processes. Mater Sci Forum 2013;765:241–4.